ELSEVIER

Contents lists available at ScienceDirect

Journal of Hazardous Materials

journal homepage: www.elsevier.com/locate/jhazmat



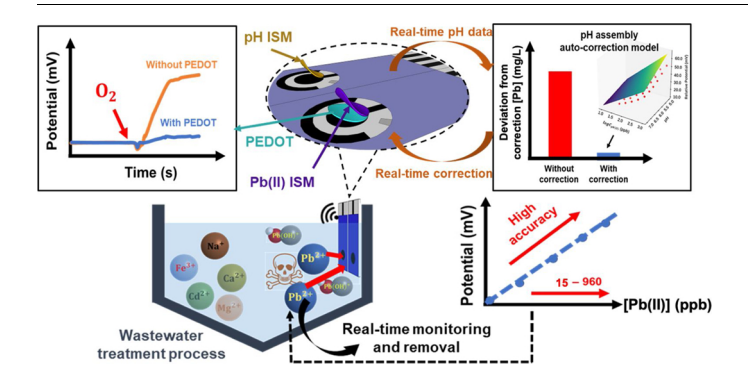
Long-term continuous and real-time *in situ* monitoring of Pb(II) toxic contaminants in wastewater using solid-state ion selective membrane (S-ISM) Pb and pH auto-correction assembly



Yingzheng Fan^a, Zhiheng Xu^a, Yuankai Huang^a, Tianbao Wang^a, Sikai Zheng^a, Alex DePasquale^a, Christian Brüeckner^b, Yu Lei^c, Baikun Li^a,*

- ^a Department of Civil & Environmental Engineering, University of Connecticut, Storrs, CT 06269-3037, United States
- b Department of Chemistry, University of Connecticut, Storrs, CT 06269-3060, United States
- ^c Department of Chemical and Biomedical Engineering, University of Connecticut, Storrs, CT 06269-3222, United States

GRAPHICAL ABSTRACT



ARTICLE INFO

Editor: D. Aga

Keywords:

Mm-sized screen-printed Pb(II) sensor
Wastewater
Conducting polymer
pH interference correction
Oxygen interference

$A\ B\ S\ T\ R\ A\ C\ T$

Lead (Pb) contaminants in wastewater have inhibited microbial activities and thus exerted high energy consumption in wastewater treatment plants (WWTPs). Current Pb monitoring has been conducted *ex situ* and off line, unable to affect real-time proactive control and operation. This study targets the crucial challenge of better and faster Pb monitoring by developing novel mm-sized screen-printed solid-state ion-selective membrane (S-ISM) Pb sensors with low-cost, high accuracy and long-term durability and that enable real-time *in situ* monitoring of Pb(II) ion contamination down to low concentrations (15 ppb–960 ppb) in wastewater. An innovative pH auto-correction data-driven model was built to overcome the inextricable pH inferences on Pb(II) ISM sensors in wastewater. Electrochemical impedance spectroscopy (EIS) and cyclic voltammograms (CV) analysis showed (3,4-ethylenedioxythiophene, EDOT) deposited onto the mm-sized screen-printed carbon electrodes using electropolymerization effectively alleviated the interferences from dissolved oxygen and improved long-term stability in wastewater. Monte Carlo simulation of the nitrification process predicted that real-time, and high accurate *in situ* monitoring of Pb(II) in wastewater and swift feedback control could save ~53 % of energy consumption by alleviating the errors from pH and DO impacts in WWTPs.

E-mail address: baikun.li@uconn.edu (B. Li).

^{*} Corresponding author.

1. Introduction

Lead (Pb) (II) has been widely used in numerous industrial applications, such as lead-acid batteries, printing pigments, fuels and photographic materials, and has been discharged into wastewater without efficient monitoring (Li et al., 2016; Zhao et al., 2012). As a highly toxic pollutant, Pb(II) adversely affects human soft tissues and organs and acts synergistically with other carcinogens at low concentrations (Andjelkovic et al., 2019; García-Lestón Julia et al., 2010; Jarosławiecka and Piotrowska-Seget, 2014; Triantafyllidou and Edwards, 2012). Pb(II) is easily bound by complex organic molecules and reduces microbial bioactivity in wastewater treatment plants (WWTPs) (Bruins et al., 2000; Zhao et al., 2012). Conventional methods for Pb(II) monitoring, such as inductively coupled plasma mass spectrometry (ICP-MS) and atomic absorption spectroscopy (AAS), possess high accuracy (Jenner et al., 1990), but they are costly and bulky and have high operator training demands. In addition, these off-line ex situ methods require water samples to be transferred from WWTPs to the laboratory, and thus causing the problems of sample quality variation and lagging times for system operation. Therefore, a low-cost, miniature and accurate Pb(II) detection method capable of real-time in situ monitoring is indispensable for swift contaminant control and energysaving in WWTPs.

Many types of Pb(II) sensors have been developed, including colorimetric, biomimetic, voltammetric, and amperometric sensors. Nevertheless, the reusability of the colorimetric sensors are poor, since they are coated with acid-capped gold nanoparticles (AuNPs) and can only be used single-time due to the irreversible aggregation of AuNPs (Kalluri et al., 2009). Biosensors such as oligonucleotide-based lead biosensors and G-quadruplex based label-free fluorescent biosensors usually possess high selectivity (Guo et al., 2012; Jarczewska et al., 2015), but their electron donors/acceptors (e.g. potassium ferrocyanide / oxygen, potassium ferricyanide) are oftentimes costly and the short lifespan of microbial cells and enzymes makes them unfeasible for continuous monitoring of Pb(II) in wastewater. Voltammetric sensors suffer from severe interferences from complex chemicals in wastewater and have poor sensitivity and selectivity for low Pb(II) concentrations (the regulated level: < 150 ppb) in wastewater (Kang et al., 2017). For instance, at Pb(II) concentrations lower than 1 µM, the sensitivity of copper-based voltammetric sensors dropped by 10 % caused by the interference with zinc (Zn) in the wastewater (Kang et al., 2017). Amperometric sensors such as G-quadruplex (G4) (Li et al., 2011) and sulfur-doped graphitic carbon lead sensors (Zou et al., 2020) exhibited a declined accuracy in wastewater. The requirement of external voltage to obtain the current readings (µA or mA) posed an obstacle for continuous monitoring in a real time mode. Furthermore, these Pb(II) sensors (e.g., Pb(II) ion optical sensors, copper-based voltammetric sensors, Co₃O₄ nanosheets Pb sensors) suffer from ill-defined but significant interference from pH, dissolved gases (particularly O2) in wastewater leading to substantial errors (Ensafi et al., 2009; Yu et al., 2017). For example, the copper-based sensors exhibited a variation of 22 % and 34 % at pH values of 5 and 4.65, respectively. Another obstacle of existing Pb(II) sensors is poor stability, mainly caused by severe contamination and fouling of the sensor surface immersed in wastewater, necessitating their frequent replacement (Bansod et al., 2017; Deng et al., 2019; Huang et al., 2014; Zou et al., 2018). Until now, long-term accuracy and stability of Pb(II) sensors in real wastewater were not achieved.

To tackle the critical challenge of Pb(II) monitoring in wastewater, this study explored an innovative mm-sized sensor using Pb(II) solid-state ion-selective membranes (S-ISM) on screen-printed carbon electrodes (SPEs), which are capable of real-time *in situ* monitoring of ultralow Pb(II) concentration (as low as 15 ppb, and up to 960 ppb) at low-cost (< \$1 each sensor), high accuracy and durability, while requiring only simple potentiometric instrumentation. To eliminate pH influences and to enhance the accuracy of Pb(II) monitoring in wastewater, an

auto-correction sensor assembly was developed by integrating Pb S-ISM sensors with pH S-ISM sensors; this was combined with an innovative data-driven model built based on a dataset of sensor readings at different pH values to compensating for the impact pH has on the Pb(II) sensor readings. Furthermore, 3,4-ethylenedioxythiophene (EDOT) was deposited onto the SPE electrodes using electropolymerization. This formed a conducting polymer layer (PEDOT) that reduces the interferences from dissolved oxygen (DO) in wastewater and prevents the formation of a water layer between the ISM and the electrode. The fundamental mechanisms of the PEDOT layer to sustain the stability of the sensor potential (mV) readings were explored through electrochemical impedance spectroscopy (EIS) and cyclic voltammograms (CV). Lastly, the long-term accuracy and mechanic stability of Pb(II) S-ISM sensor was examined in real wastewater. Hydrophobicity of sensor surface was monitored over time and correlated with the sensor electrochemical and anti-fouling performance. The capability of the Pb(II) S-ISM sensor to capture transient Pb(II) shocks at different pH and DO were also examined in real wastewater.

This study consisted of six individual tasks: First, novel mechanically stable screen-printed S-ISM sensors were developed for monitoring Pb(II) and pH. Linear correlation between the sensor potential readings (mV) and the ultra-low concentration of Pb(II) (< 150 ppb) was established. Second, accuracy and selectivity of the Pb(II) S-ISM sensors in the presence of competing ions in different types of aqueous solutions were examined. Third, the pH influence on the Pb(II) S-ISM sensor was determined and an auto-correction data-driven model was built to eliminate the pH influence. Fourth, a conducting polymer PEDOT was deposited onto the carbon electrode surface to enhance the sensor reading stability in wastewater. The fundamental mechanisms of PEDOT to minimize DO impacts were explored through EIS and CV analysis. Fifth, the long-term stability of Pb(II) S-ISM sensors were examined in real wastewater over a 2-week period. Lastly, a stochastic and Monte Carlo simulation was built to predict the energy-saving in WWTPs as a consequence of the accurate real-time in situ Pb(II) S-ISM

2. Materials and methods

2.1. Fabrication of Pb(II) and pH solid-state ion selective membrane (S-ISM) sensors with PEDOT layer

The overall sensor (length: 3.5 cm, width: 1.5 cm, height: 0.1 cm) was fabricated by screen printing technology (SPT) (Fig. 1a). A conducting polymer, poly(3,4-ethylenedioxythiophene) (PEDOT) was coated onto the carbon-based working and reference carbon-electrodes (radii: 1.5 mm) using galvanostatic electrochemical polymerization in a de-aerated aqueous solution containing 0.01 M EDOT (Sigma-Aldrich) and 0.1 M supporting electrolyte poly(sodium 4-styrenesulfonate) (NaPSS) (Sigma-Aldrich). A constant current of 0.014 mA (0.2 mA/cm²) was applied for 714 s in the polymerization process in order to produce a polymerization charge of 10 mC (Bobacka, 1999). The PEDOT layer was dried on the electrode surface under the room temperature for around 12 h.

Subsequently, the Pb(II) ISM mixture consisting of liquid-state Pb (II) ionophore IV (tert-butylcalix[4]arene-tetrakis(N,N-dimethylthioacetamide) – 5 wt%) (Sigma-Aldrich), o-NOPE (2-nitrophenyloctylether – 48 wt%) (Sigma-Aldrich), NaTFPB (sodium tetrakis[3,5-bis(trifluoromethy)phenyl]borate – 2 wt%) (Sigma-Aldrich) as the cation exchange component and PVC (polyvinyl chloride – 45 wt%) (Sigma-Aldrich) as the supporting polymer. This ISM mixture was first dissolved in 500 μL of tetrahydrofuran (THF); then 4.5 μL of this mixture solution was carefully drop-cast on the top of the PEDOT layer of the working carbon-electrode (radius: 1.5 mm) and dried on the electrode surface in a sealed container filled with N_2 at room temperature over 24 h to form the solid-state ISM (S-ISM) sensor.

The pH sensing membrane consisted of liquid-state hydrogen

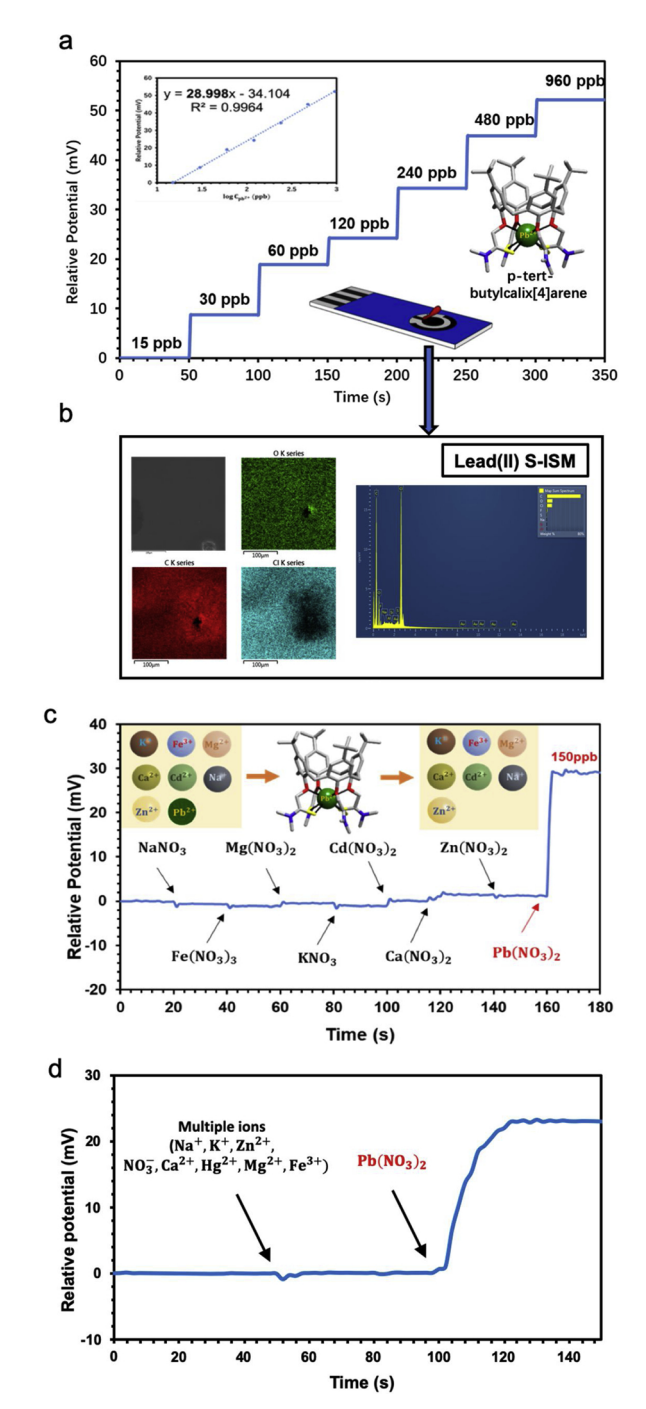


Fig. 1. (a) The calibration curve of the Pb(II) S-ISM sensor at different Pb(II) concentration (15 ppb to 960 ppb) (Insert: the structure the Pb(II) ionophore tert-butylcalix[4]arene-tetrakis(N,N-dimethylthioacetamide)). (b) The EDS image of Pb(II) S-ISM and atomic percentage. (c) Selectivity test for the Pb(II) S-ISM sensor by adding interference metal ions sequentially. (d) Selectivity test for the Pb(II) S-ISM sensors by adding interference metal ions and Pb(II) ions simultaneously.

ionophore V (tert-butylcalix[4]arene-tetrakis(N,N-dimethylthioacetamide) - 10 wt%) (Sigma-Aldrich), o-NOPE (2-nitrophenyloctylether -89.3 wt%) (Sigma-Aldrich), and NaTFPB (sodium tetrakis[3,5-bis(trifluoromethy)phenyl]borate - 2 wt%) (Sigma-Aldrich). This mixture was first dissolved in 500 µL of tetrahydrofuran (THF) and 4.5 µL of this solution solution was carefully drop-cast on the top of the PEDOT layer of the working carbon-electrode (radius: 1.5 mm). The drying procedure of the pH ISM mixture was the same as for the Pb(II) sensor.

Then, the pH S-ISM sensor was calibrated in pH buffer solutions in the range from pH 5 to 9. The potential (mV) readings of the pH sensor were recorded for each pH buffer solution using an electrochemical working station (CHI 660D).

Surface characterization of the Pb(II) S-ISM sensor was achieved using a scanning electron microscope (SEM) (FEI Nova NanoSEM 450), after sputter-coating with gold-palladium layer (Polaron E5100 Sputter Coater) for 2 min, and equipped with an Energy Dispersive X-ray Spectroscopy (EDS) Microanalysis Equipment (Oxford AZtecEnergy Microanalysis System with X-Max 80 Silicon Drift Detector).

2.2. Calibration and selectivity tests of Pb(II) S-ISM sensors

Pb(II) S-ISM sensors were calibrated in aqueous solutions (Pb(II) concentration: 15, 30, 60, 120, 240, 480-960 ppb) by sequentially adding Pb(NO₃)₂ concentrated solution (1000 ppb) into 100 mL deionized water every 50 s. The pH of the water solution was maintained at 5.0 to prevent the precipitation of Pb(OH)2. The potential (mV) readings of the Pb(II) S-ISM sensor was recorded using the electrochemical working station (CHI 660D).

Selectivity of the Pb(II) S-ISM sensor was examined in a water solution by sequentially adding different non-target ions, including KNO₃ (150 ppb), Fe(NO₃)₃ (150 ppb), Mg(NO₃)₂ (150 ppb), Ca(NO₃)₂ (150 ppb), Cd(NO₃)₂ (150 ppb), NaNO₃ (150 ppb), Zn(NO₃)₂ (150 ppb). After adding the interfering salt solutions, a Pb(NO₃)₂ solution (150 ppb) was injected to examine whether the Pb(II) S-ISM sensor exhibited the accurate potential (mV) response. In a parallel test, these non-target ions and Pb(NO₃)₂ in the aforementioned concentration range were simultaneously added into a water solution and then the sensor readings were recorded.

2.3. Developing auto-correction data-driven model to determine the pH influence on Pb(II) S-ISM sensors

Due to constant variations of pH values in WWTPs, the pH-dependent readings of the Pb(II) sensor should be corrected frequently to minimize the measurement errors. In this study, the readings of Pb(II) S-ISM sensors were first obtained under a series of Pb(II) concentrations (15, 30, 60, 120, 240, 480-960 ppb) at different pH values (5, 5.5, 6, 6.5 and 7). The pH of these solutions was monitored using the pH S-ISM sensors in a real-time mode. The potential (mV) readings of both Pb(II) and pH S-ISM sensors were integrated to fit a regression model using the Minitab program, through which three variables (Relative Potential: ΔE, pH value and Pb(II) concentration) were integrated into a pH autocorrection model. The pH auto-correction model was then described in 3-D figures using the Python Matplotlib Program.

The pH auto-correction model was verified in simulated wastewater by measuring Pb(II) concentrations (60 ppb and 120 ppb) with pH ranging from 5.0-7.0. The measurement errors of these two Pb(II) concentrations with the pH auto-correction model were compared with the corresponding errors without the pH-auto-correction model (as a control).

2.4. Examination of the impact of dissolved oxygen (DO) on Pb (II) S-ISM sensor

The Pb(II) S-ISM sensor with the PEDOT conducting polymer layer was examined in a beaker (volume: 200 mL) holding a water solution (Pb(II) concentration: 150 ppb) saturated with dissolved oxygen (DO: 9 mg/L) through aeration (Shi et al., 2015). The performance was compared side-by-side with a Pb(II) S-ISM sensor without PEDOT (as a control) deployed in the same beaker. The potential readings (mV) of both sensors were recorded simultaneously at an interval of 1 s using the electrochemical working station (CHI 660D). During the test period, O₂ was continuously pumped into the water solution for around 50 s.

Electrochemical impedance spectroscopy (EIS) and cyclic

voltammograms (CV) were performed to characterize the electrochemical property of the printed carbon electrodes (with and without PEDOT) in the aerated solution. Specifically, EIS was conducted in a 0.1 M KCl solution at the reference electrode potential of 0.2 V. The results were recorded in the frequency range 100 kHz to 0.1 Hz by using an excitation amplitude (ΔE_{ac}) of 10 mV before and after pumping oxygen. CV was performed in the potential range 0.5 to -0.5 V at a scan rate of 0.1 V/s in 0.1 M KCl solutions before and after pumping oxygen.

2.5. Long-term stability test of Pb(II) S-ISM sensors in wastewater

Long-term stability of Pb(II) S-ISM sensors was examined by immersing three sensors fabricated in the same batch into an aqueous solution (Pb(II): 150 ppb) for 2-week period. The readings (mV) of these three sensors were compared to reflect the variations of sensitivity. Every three days, Pb(II) S-ISM sensors were taken out of the water solution and calibrated at different Pb(II) concentrations (ranging from 15 ppb to 960 ppb), through which the long-term accuracy and sensitivity of these sensors were determined over the 2-week period. In the meantime, the morphology of the Pb(II) S-ISM sensors was observed weekly using a scanning electron microscope (SEM) (FEI Nova NanoSEM 450). The hydrophobicity of the Pb(II) S-ISM surface was examined by measuring the contact angle using the CAM 101 optical surface tension meter (KSV Instrument Inc.).

2.6. Capturing transient shocks in real wastewater

Transient shock tests were performed by adding a highly concentrated Pb(NO₃)₂ solutions (1000 ppb) twice in a container (volume: 100 mL) holding real wastewater collected from the Wastewater Treatment Plant at the University of Connecticut. The Pb(II) concentration in wastewater was measured by the Salicylate Method (Method 850) using Hach DR2800. The theoretical Pb(II) concentration in the container after transient shocks was calculated based on the initial concentration and the injected volume of the Pb(NO₃)₂ shock solution. Consequently, the pH of the solution in the container was expected to change due to the addition of the Pb(NO₃)₂ shock solution. The Pb(II) S-ISM sensor in the container was examined to capture the prompt potential change of the Pb(II) concentrations. Auto-correction model was applied to compensate the pH impact. The result with pH auto-correction was side-by-side compared with the one without pH auto-correction (as a control) to examine the accuracy of the pH autocorrection data-driven model.

3. Results and discussion

3.1. Calibration and selectivity of Pb(II) S-ISM sensors in simulated wastewater

The solid-state ion selective membrane (S-ISM) contains critical sensing functionalities with the main elements of C, O and Cl at the atomic percentage of 83.52 %, 10.57 % and 4.41 %, respectively (the Energy Dispersive X-ray Spectroscopy (EDS) image (Fig. 1b). For the mm-sized screen-printed Pb(II) S-ISM sensor, the detection limit as the intersection of the two slopes was 2 ppb (Fig. S1) in wastewater, which is substantially improved over that limit reported for a polypyrrole-Zr (IV) Pb(II) selective electrode (detection limit: 662.4 ppb) and Pb(II)-ISE electrode based on GC/ISM (detection limit: 82.4 ppb) (Jiang et al., 2019; Khan et al., 2016). A previous study found that detection limit was positively associated with the transmembrane fluxes of the target ion (e.g., Pb(II) in this study) (Püntener et al., 2004). The thickness of the Pb(II) ISM was increased in this study by applying higher supporting polymer ratios (45 wt%) to lower transmembrane ion flux (Lisak et al., 2012), thus leading to a better detection limit.

Calibration tests were conducted in aqueous solutions with Pb(II) concentrations ranging between 15 and 960 ppb, including the

regulated Pb(II) concentrations in drinking water (15 ppb) and wastewater (150 ppb) (EPA, 2017). The pH value (pH \leq 5) was controlled using nitric acid (HNO₃) to prevent Pb(II) precipitation (Sari et al., 2007; Wang et al., 2009). According to the Nernst equation, an excellent linear relation was obtained with a Nernstian slope $(k_{Pb(II)} = \frac{2.3026 \times RT}{r})$ of 28.998 per decade of Pb concentration $(R^2 > 0.99)$ (Fig. 1a), which was close to the ideal Nernstian response for divalent cations (29 mV per decade) (Bu, 1998). This sensitivity was higher than the Pb(II) sensors previously reported (polypyrrole-Zr(IV) phosphate Pb (II) selective sensor: 26.37 mV dec⁻¹, graphene Th(IV) Pb(II) selective sensor: 27.65 mV dec⁻¹) (Khan et al., 2016; Rangreez and Inamuddin, 2016). We ascribed the higher affinity of the chelate *p-tert*-butylcalix[4] arene (Fig.1a) used containing the soft sulphur donor atoms with a high affinity for the soft Pb(II) cations, combined with a large enough cavity of the calix[4] arene to fit the large Pb(II) cations (119 pm) (Lisak et al., 2013).

Wastewater contains numerous types of ions and poses severe interference for real-time *in situ* monitoring of Pb(II). In order to eliminate measurement errors generated from the high chloride contents (5000–10000 mg/L) in wastewater (Rajkumar et al., 2007), the Ag/AgCl reference electrode normally used in water sensors (Polk et al., 2006) was replaced in this study by a screen-printed carbon reference electrode. The accuracy of the screen-printed carbon reference electrode was compared with the Ag/AgCl reference electrode in aqueous solutions of NaCl (Cl⁻ concentration: 5–50 mg/L). The potential readings (mV) of the carbon reference electrode were invariant with the presence of chloride, whereas the readings of the Ag/AgCl reference electrode deviated strongly in the presence of chloride (Fig. S2).

To determine the electivity of our Pb(II) sensor, different monovalent, bivalent and trivalent metal ions commonly present in wastewater such as Na(I), Fe(III), Mg(II), K(I), Cd(II), Ca(II), Zn(II) were sequentially added into an aqueous solution. The potential (mV) reading of the Pb(II) sensor was only little affected by these interfering metal ions (Fig. 1c). In contrast, when the targeted Pb(II) ion was added into the water solution, the mV readings of the S-ISM sensor responded sharply and promptly (within 5 s) (Fig. 1c). This response time is much faster than that of sensors in previous studies (polyphenylenediamine lead electrode (Huang et al., 2011) and 2,2'[propane-1,3-diylbis(oxy)] dibenzaldehyde Pb(II) electrode (Kaur and Aulakh, 2018). This excellent selectivity was ascribed to the lipophilic ion-exchanger sodium tetrakis[3,5-bis[trifluoromethy]pheyl]borate (NaTFPB) present in the membrane and the cavity of calix[4]arene in Pb(II) S-ISM sensor (Pechenkina and Mikhelson, 2015), which lowered the membrane resistance of neutral carrier-based electrodes and only accommodate the dimension of Pb²⁺ cations (119 pm), respectively. Compared with other Pb(II) ionophores (e.g., tertiary amide, diaza-crown ethers and pyridinecarboxy-imide), p-tert-butylcalix[4]arene offered dual features (polar: lower rim; non-polar: upper rim) that could effectively enhance the selectivity towards Pb(II) over other metal ions (Yang et al., 2015). It should be noted that Ag(I) cations (at a concentration of 150 ppb) also interfered with the potential (mV) readings of Pb(II) S-ISM sensors (Fig. S3) since its affinity of the thioamide derivatives for this also also soft and large ion is also high (Kulesza and Bocheńska, 2011). However, the concentration of Ag(I) in municipal wastewater is normally too low (1 ppb ~ 40 ppb) (Kühr et al., 2018) to affect the Pb(II) sensors. Furthermore, in a parallel test that all the non-targeted ions were simultaneously added along with Pb(II), the Pb(II) S-ISM sensor still exhibited the excellent selectivity to explicitly capture the target Pb(II) ion without the minimal interference of these non-targeted ions (Fig. 1d), ensuring the high selectivity of the Pb(II) S-ISM sensors with the presence of numerous non-targeted ions in wastewater.

3.2. pH influence on the accuracy of Pb(II) monitoring

In WWTPs, the pH values vary frequently due to influent variations

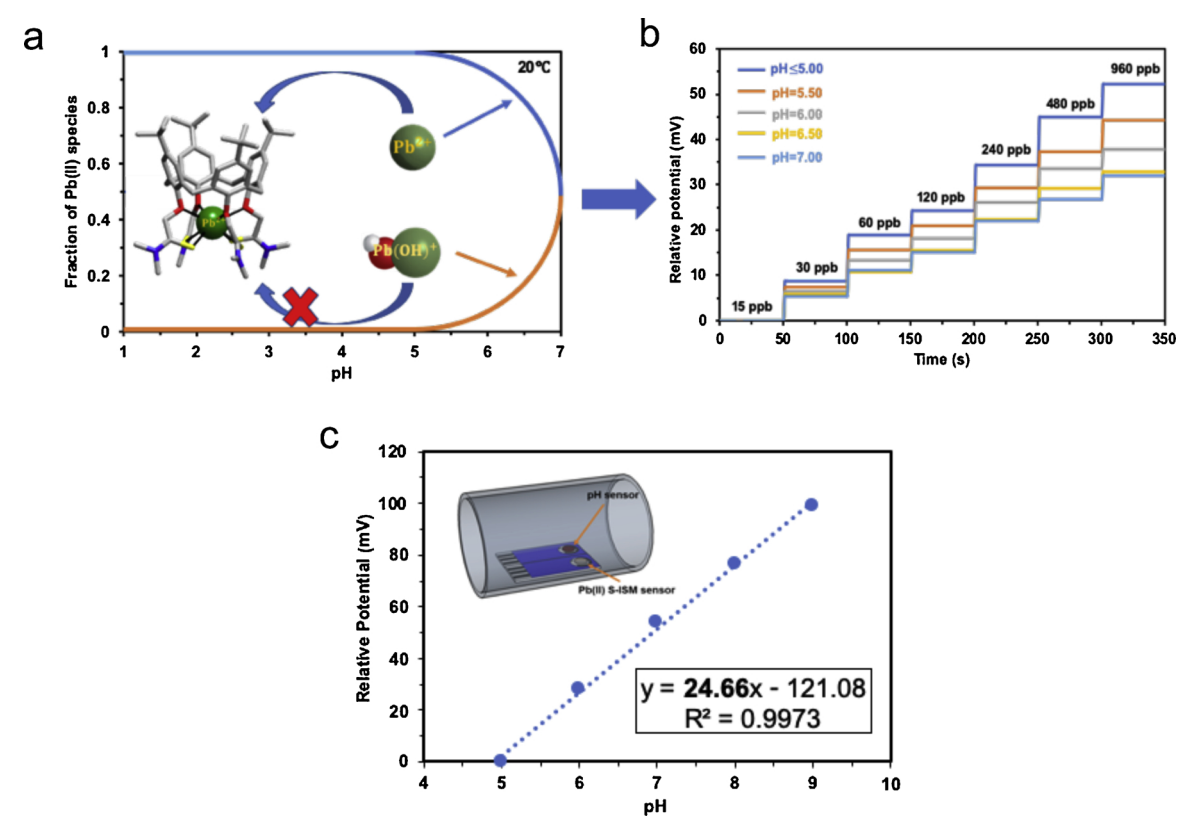


Fig. 2. (a) The hydrolysis process of Pb(II) ions (Pb²⁺ and PbOH⁺) at pH range from 1.00 to 7.00. (b) The potential-time ladder for the Pb(II) S-ISM sensor at different Pb(II) concentration (15 ppb to 960 ppb) with the pH range from 5.00 to 7.00. (c) The calibration curve of the integrated pH sensor at different pH values from 5 to 9.

and different biochemical reactions (e.g., nitrification, denitrification and anoxic reactions) (Chua et al., 2003). pH variation in wastewater has caused severe measurement error for Pb(II) monitoring (Huang et al., 2017; Liu et al., 2019; Rozendal et al., 2008) since at high proton concentrations, the protons directly compete with Pb(II) ions for bonding with the ionophore. At relatively lower proton concentrations $(5.00 \le \mathrm{pH} \le 7.00)$, the large variation in the potential (mV) response with the pH values is caused by the change of the speciation of the Pb (II) ions (Sari et al., 2007; Wang et al., 2009):

$$Pb^{2+} + OH^{-} = PbOH^{+}$$
 (1)

$$K_1 = \frac{[PbOH^+]}{[Pb^{2+}][OH^-]}$$
 (2)

At low pH (\leq 5.00), the total Pb(II) concentration exists in the form of 'free' Pb2+ ions (Fig. 2a). When pH value reached to 5.0, hydroxylated Pb(II) complexes started to form, thus the total Pb(II) concentration consist of the species Pb2+ and PbOH+. The formal deprotonation of the hydrated Pb(II) ions began at pH value above 5.00-7.00 (Fig. 2a). However, the cavity of calix[4] arene only fits the dimension of Pb²⁺ cations (119 pm), while PbOH⁺ (269 pm) is unable to enter into the cavity of calix[4] arene, resulting in a reduced sensitivity (Fig. 2a). The variation of sensitivity with pH values verified that the Pb²⁺ S-ISM sensor could only capture Pb2+ ions rather than the total Pb(II) species (Pb²⁺ and PbOH⁺). The Nernstian slope of Pb(II) concentration dropped by approximately 38 % when pH value increased from 5.0-7.0 (Fig. 2b), again showing that the Pb(II) S-ISM sensor became inaccurate to monitor the total Pb(II) at pH higher than 5.0. At pH higher than 7.00, Pb(OH)₂ precipitation sets in, as performed also in conventional Pb-removal methods (Marani et al., 1995). Previous studies also found the pH influence deteriorated the accuracy of ISM sensors (Li et al., 2009; Liu et al., 2019). Until now, there has been no sensor material or effective method capable of eliminating the pH influence on Pb(II) sensors.

3.3. Developing auto-correction data-driven models to minimize pH impact

An auto-correction sensor assembly was developed by integrating a pH S-ISM sensor with the Pb(II) S-ISM sensor to compensate the pH influence (Fig. 2c). The readings of Pb (II) and pH sensors under a series of concentrations of Pb(II) (in the range from 15 to 960 ppb) and pH (5.0–7.0) were continuously fed into a data-driven model. The results showed that there was an excellent linear relationship between potential (mV) and pH values (R² value: 0.9973) at the pH range of 5–7, allowing a real-time pH monitoring and correction (Fig. 2c).

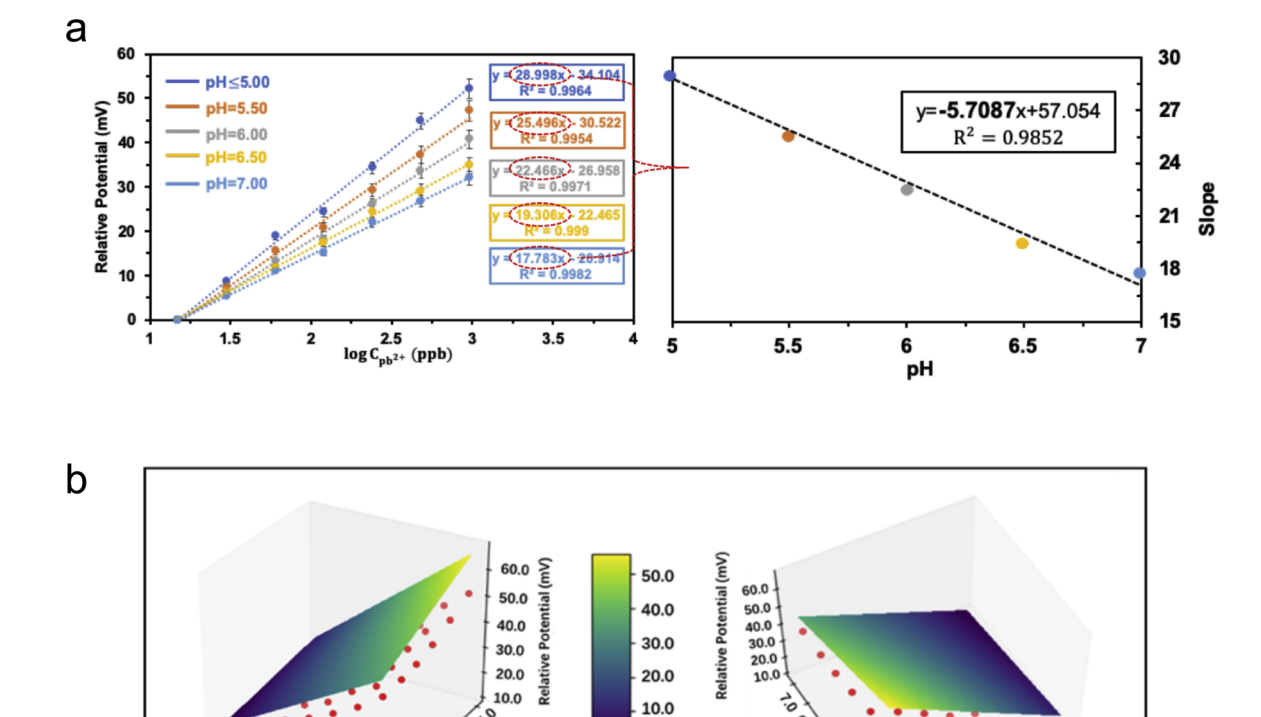
For the Pb(II) S-ISM sensor, Nernstian slopes of different pH values possessed an excellent linear relation with its corresponding pH ($R^2 > 0.98$) (Fig. 3a), based on which a model between the slope and the pH was established (Eq. 3):

$$k_{Pb(II)} = k_{pH} \cdot pH + \alpha \tag{3}$$

Where $k_{Pb(II)}$ is the Pb(II) Nernstian slope under various pH values, k_{pH} is the pH coefficient, α is the pH adjustment coefficient. Based on this relationship of the slope of the Pb(II) S-ISM sensor and pH, an autocorrection data-driven model could be built for the relative potential response (ΔE , mV) of the Pb(II) S-ISM sensor under two variables (pH and Pb(II) concentration) by fitting all the data into the Nernstian equation (Eq.4).

$$\Delta E = k_{pH} \cdot pH \cdot log_{10} C_{Pb(II)} + \alpha \cdot log_{10} C_{Pb(II)} + \beta$$
(4)

Where $C_{\text{Pb(II)}}$ is the concentration of Pb(II) in water sample, pH is the pH value in a water solution, ΔE is the relative open circuit potential (OCP) generated by the Pb(II) S-ISM sensor, β is the adjustment coefficient for the auto-correction model. This auto-correction model ($\Delta E = -2.668 \cdot \text{pH} \cdot \log_{10} C_{\text{Pb(II)}} + 38.82 \cdot \log_{10} C_{\text{Pb(II)}} - 26.99$) was plotted using the Python code, in which the red dots were the original data of the Pb(II) S-ISM sensor and the green flat plane was the auto-corrected values regressed from the model (Fig. 3b). The details of this Python



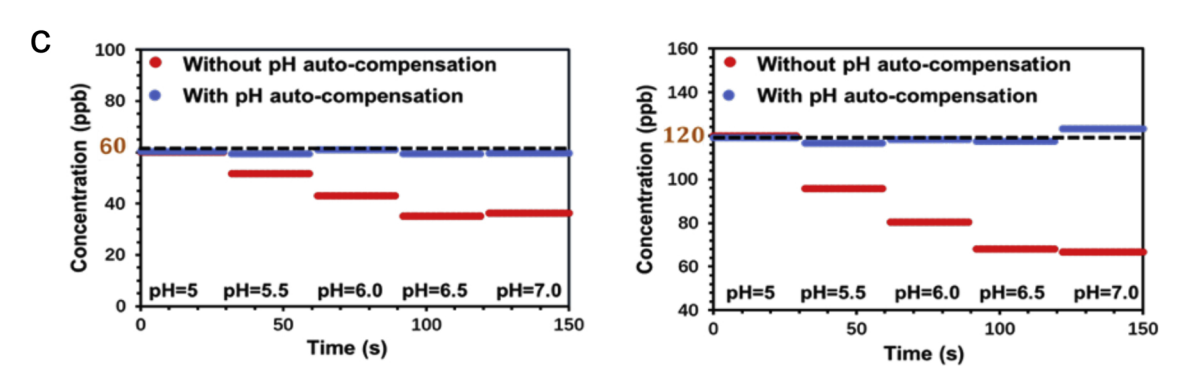


Fig. 3. (a) The calibration curve of the Nernstian slopes at different pH values (5.00 to 7.00). (b) The 3D plot of the fitted auto-correction model (plane) based on the Pb(II) sensor data in the range for Pb(II) concentration (15 ppb to 960 ppb) and pH (5.00 to 7.00). (c) Performance comparison of the Pb(II) S-ISM sensor with pH correction and without correction (as a control) at the pH range from 5.00 to 7.00 for two different Pb(II) concentration (60 ppb and 120 ppb).

codes for the auto-correction data-driven model were shown in Table S1. The regression values almost covered all of the original sensor data with a high R^2 value of 0.9862, demonstrating an excellent fitted 3-D regression, through which the Pb(II) concentration in water solution could be accurately predicted based on the relative potentials of the Pb (II) and pH sensors.

b(II) (Ppb)

In order to evaluate the accuracy of the pH auto-correction model, a validation test was performed by measuring Pb(II) concentrations (60 ppb and 120 ppb) in simulated wastewater of pH ranges between 5.0 and 7.0. The measurement errors of of the uncorrected measurements at 60 ppb and 120 ppb Pb(II) concentration at the pH of 7.0 was as large as 44 % and 39 %, respectively. In contrast, the measurement error obtained for the Pb S-ISM sensor for which the correction model was applied at a pH of 7.0 was only 0.5 % (60 ppb) and 2.6 % (120 ppb) (Fig. 3c), satisfying the error requirement of the EPA (< 5%). These

results demonstrated the efficiency of using the pH auto-correction model to correct the large deviation of the Pb(II) S-ISM sensor readings under different pH values in wastewater.

3.4. The influence of dissolved oxygen on Pb monitoring

Dissolved oxygen (DO) in wastewater is essential to sustain microbial activity to degrade contaminants in WWTPs (Changqing et al., 2011; Holenda et al., 2008). But DO causes potential (mV) reading errors of the Pb(II) S-ISM sensor (Fig. 4a). One effective approach to stabilize the electrochemical sensor readings under fluctuating oxygen environments is to apply an electroactive polymer as the ion-to-electron layer due to its high electrical conductivity and capacitance (Meng et al., 2017; Naveen et al., 2017). Electrical conductivity is closely associated with the ion-to-electron transduction competence, which is

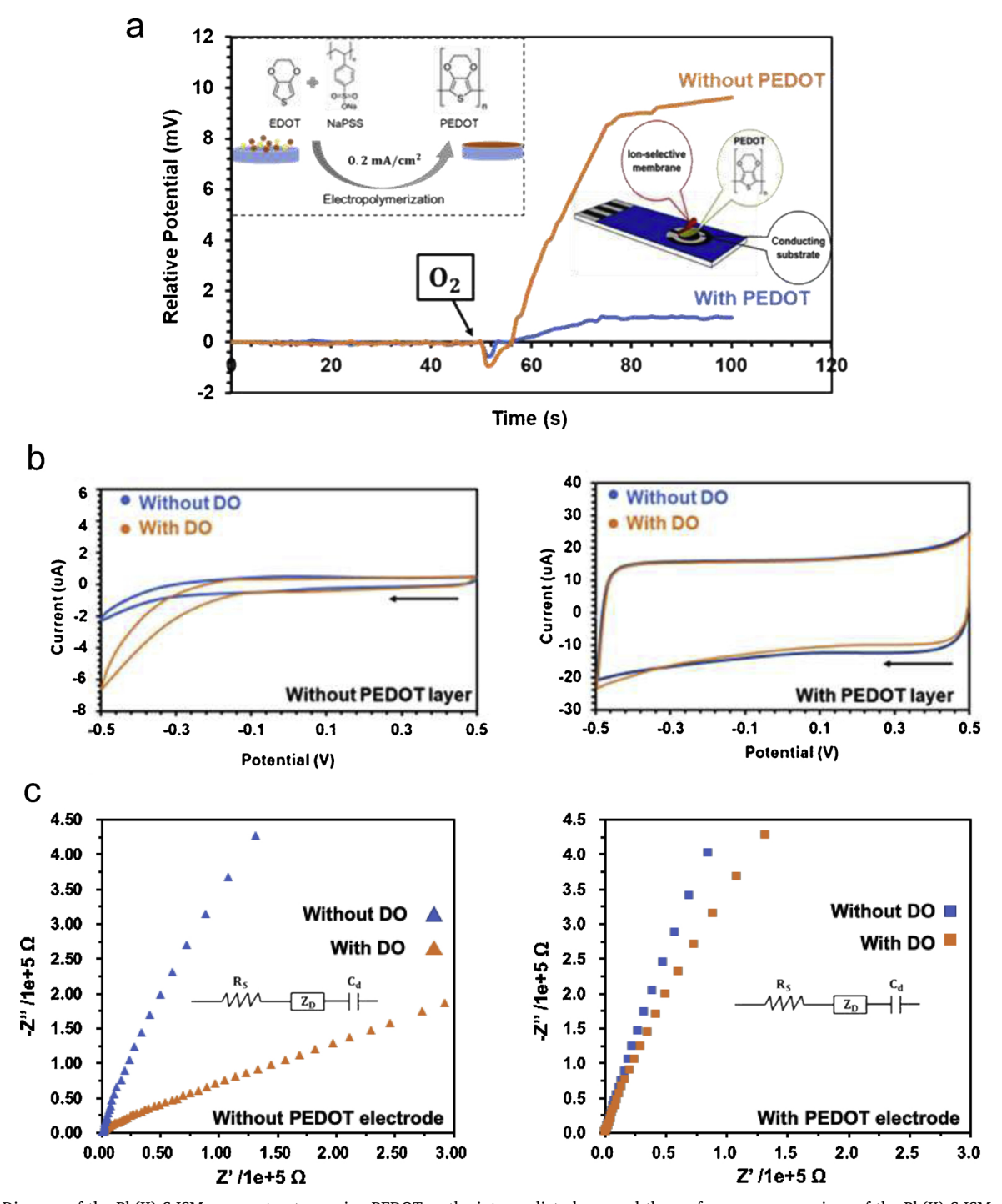


Fig. 4. (a) Diagram of the Pb(II) S-ISM sensor structure using PEDOT as the intermediate layer and the performance comparison of the Pb(II) S-ISM sensor with PEDOT layer and without PEDOT layer (as a control) in the presence of interfering dissolved oxygen. (b) The cyclic voltammetry test of the printed carbon electrodes with PEDOT layer and without PEDOT layer (as a control) in the presence of interfering dissolved oxygen. (c) The electrochemical impedance spectroscopy (EIS) test of the printed carbon electrode with PEDOT layer and without PEDOT layer (as a control) in the presence of interfering dissolved oxygen.

determined by the band gap of the materials (the energy difference between the valance band and the conduction band). Compared with other conducting polymers such as polypyrrole (PPy) (band gap: 3.1 eV), poly(phenylene vinylene)s (PPV) (2.5 eV) and polyaniline (PANI) (3.2 eV), PEDOT possesses a much lower band gap (1.1 eV), which contributes to its high conductivity (300 S/cm) (Moon et al., 2018; [nullS]). Thus, PEDOT was chosen in this study as the intermediate layer deposited onto the screen-printed carbon electrode so as to alleviate the DO interference towards Pb(II) S-ISM sensors (Fig. 4a).

The potential (mV) readings of the Pb(II) S-ISM sensor without

PEDOT deposit (as a control) drifted by 9.61 mV after aerating an aqueous $Pb(NO_3)_2$ solution for 50 s (DO: 9 mg/L, saturation) (Fig. 4a). In contrast, the readings of the Pb(II) S-ISM sensor with the PEDOT intermediate layer only changed by 0.72 mV after aeration. In order to quantify the DO impact on the electrode potential, cyclic voltammograms (CV) of the printed carbon electrode (with and without PEDOT deposit) were recorded under oxygen saturation conditions. After pumping oxygen, a prominent reduction peak was displayed around -0.5 V that attributed to the oxygen reduction onto the electrode surface (without PEDOT deposit) (Fig. 4b). However, after covering the

electrode with a PEDOT layer, the oxygen reduction on the electrode only showed a slight current deviation in the scan range from 0.5 V to -0.5 V. From this point, the PEDOT obviously possessed a small catalytic effect on the reduction of oxygen. Meanwhile, according to previous study (Bobacka et al., 2000), the charge (Q_{cv}) was obtained by integration of the CV in the potential range from -0.5 to 0.5 V:

$$Q_{cv} = \frac{Q_a + Q_c}{2} \tag{5}$$

Where Q_a and Q_c are the anodic and cathodic charges, respectively. The charge (Qcv) of the voltammograms for the electrode without PEDOT layer before and after pumping oxygen had a difference of 58.6 %, while the sensor with the PEDOT intermediate layer only had the difference of 2.9 % (Fig. 4b), demonstrating that PEDOT deposition was quite effective to reduce the influence of DO. In addition, there was almost no high-frequency semi-circle observed in the electrochemical impedance spectroscopy (EIS) analysis of printed carbon electrodes (Fig. 4c), indicating a fast charge transfer at the carbon electrode PEDOT and PEDOT solution interfaces. The EIS results were fitted to the equivalent circuit model (Fig. 4c), composed of the solution resistance (R_s) , the capacitance (C_d) and the finite-length Warburg diffusion element (Z_D) . Based on the equivalent circuit model, the capacitance of the carbon electrode with covering PEDOT was around 258 μF , which was obviously larger than the one without covering PEDOT (12.6 μF , Fig. 4c), indicating that PEDOT increased the capacitance of the electrode. In terms of sensor reading stability, data drift ($\Delta E/\Delta t$) was associated with low-frequency capacitance (C) and its current (i), described as (Bobacka, 1999):

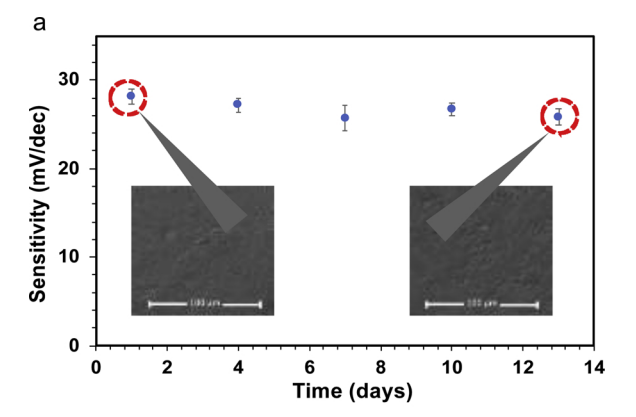
$$\frac{\Delta E}{\Delta t} = \frac{i}{C} \tag{6}$$

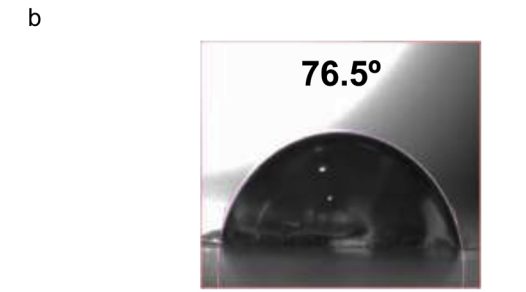
To minimize data drifting (low $\frac{\Delta E}{\Delta t}$) and enhance the reading stability of the sensor, the capacitance (C) of the electrode should be increased. Meanwhile, based on the equivalent circuit model (Fig. 4c), the aeration process obviously increased the solution resistance from 130.1 Ω to 224.9 Ω for the electrode without PEDOT layer, while for the electrode with PEDOT layer it only slightly increased the solution resistance from 145.2 Ω to 158.1 Ω . Thus, the PEDOT layer was suited to alleviate the reduction effect generated by the oxygen for the iontransport process from solution to electrode surface. With regard to the influence of dissolved carbon dioxide (CO₂), it altered the pH of water solution (Cohen and Kirchmann, 2004) and thusly interfered with traditional Pb(II) sensors. The pH auto-correction data-driven model developed in this study also effectively compensates the pH impact associated with dissolved CO₂.

3.5. Long-term stability of Pb (II) S-ISM sensors in wastewater

Long-term stability is of the primary concern for the accurate Pb(II) monitoring in WWTPs. Sensors in wastewater particularly face severe challenges incurred from complex chemical and biological pollutants (biofouling) on the sensor surface (Lee et al., 2006). For example, the commercial ISM sensors were unable to continuously monitor wastewater even for 20–30 min, suffering from severe fluctuation and reading drifting mainly due to the biofouling, and had to be taken out from wastewater every 30 min for cleaning by manually paper-wiping sensor surface, meaning that the monitor could only be used as an intermittent one-point measurement device and/or a calibration device for wastewater monitoring.

Thus, long-term stability tests were conducted using real wastewater in this study. The results showed that the sensitivity of the Pb(II) S-ISM sensor sustained around 26-29 mV per decade of Pb(II) concentration for two weeks in wastewater (Fig. 5a). Previous studies had found sensors lost almost half of its Nernstian response slope over this time (Ensafi et al., 2009; Lee et al., 2006). The readings of three pieces of sensors tested had slight deviations (< 3 mV dec $^{-1}$) (Fig. 5), which





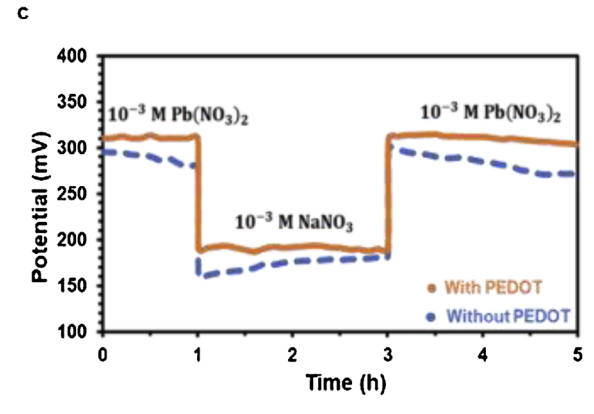


Fig. 5. (a) Long term test of the Pb(II) S-ISM sensor over two weeks (Insert: SEM images of the Pb(II) S-ISM surface before and after two weeks). (b) The contact angle test of the Pb(II) S-ISM sensor surface. (c). Aqueous-layer test for the carbon/Pb(II)-ISM without PEDOT (as a control) and carbon/PEDOT/Pb(II)-ISM electrodes switched between Pb(NO₃)₂ solution and NaNO₃ solution.

was likely a result of the manual drop-casting fabrication procedure and the resulting disparity of S-ISM sensor layer thickness. Mass production using auto-casting devices will likely achieve better quality control and more consistent readings among different sensor specimen. Furthermore, the SEM images showed that the surface morphology of the Pb(II) S-ISM sensors did not change visibly (e.g. no bacterial attachment) throughout the 2-week immersion period (Fig. 5a).

Four main reasons might contribute to the good long-term stability and sensitivity of the Pb(II) S-ISM sensors. First, the cation exchange component (sodium tetrakis[3,5-bis(trifluoromethy)phenyl]borate) of S-ISM improved the selectivity of the sensor by enhancing its capability of exchanging cations with the aqueous phase, which served as a filter to reduce the interferences from anions (Guziński et al., 2013). Second, the plasticizer (e.g., 2-nitrophenylocty ether) improved the elasticity to the PVC polymer matrix and the overall mechanical and chemical stability of the S-ISM membrane (Gupta et al., 2002). The moderate hydrophobicity (contact angle: 76.5° < 90°) of the ISM surface reduced

the biofouling possibility in wastewater (Fig. 5b). Third, the presence of an aqueous-layer between ISM and electrode surface was found to deteriorate the sensor stability when the tested solution was changed (Fibbioli et al., 2000). To validate this concept for the sensors developed in this study, aqueous-layer tests were conducted by switching the sensors between a solution containing the targeted ion and a solution containing the non-targeted interference ions and then check whether the potential (mV) readings of the sensors changed during this switch. The results showed that the Pb(II)-ISM electrodes without PEDOT (as a control) clearly showed a potential (mV) drift when the solution containing Pb(II) ions was change to the solution containing Na(I) (Fig. 5c), an interfering ion, since the primary ion (Pb(II)) was slowly replaced by the interfering ion in the S-ISM layer as the consequence of water penetration onto the electrode surface. In contrast, the Pb(II) S-ISM electrodes with the PEDOT layer showed a stable potential under the similar solution change (Fig. 5c), indicating that the PEDOT layer tightly deposited using electropolymerization effectively enhanced the bond between S-ISM and electrode surface, and alleviated the aqueouslayer formation between the S-ISM and the electrodes (Yu et al., 2011). Fourth, zwitterionic PEDOT (NaPSS + EDOT) coated on the carbon reference electrode (Fig. S4) could reduce fouling problem in wastewater, since the surfactant NaPSS possessed the amphiphilic nature capable of preventing bacterial attachment onto the electrode surface (Yang et al., 2012), and thus alleviate the fouling of the reference electrode and ultimately prolonged the stability of the Pb(II) S-ISM sensors.

Main features of mm-sized S-ISM Pb(II) sensor were extensively compared with Pb(II) sensors reported previously (Table 1). Specifically, Schiff base (Jeong et al., 2005a) and sol-gel (Ardakani et al., 2005) Pb(II) sensors possessed good sensitivity (29.4 and 28.9 mV dec⁻¹), while their selectivity was compromised and interfered by the same charge ions (e.g., Cu(II)) that form strong complex with the Pb(II) ionophores used. Commercial ISM sensor (TruLine Lead Electrode Kit. n.d.2020) and single-piece nanocomposite (Liu et al., 2019) Pb(II) electrodes have a good response time (~10 s) due to their thin film and the enhanced ion flux into the membranes. However, high ion flux easily caused unstable sensor readings under fluctuating environments (e.g., DO concentration variation). Optical-sensing film Pb(II) sensors possessed good stability in clean water solution due to durable entrapment of optical chemosensors (Ensafi et al., 2009). However, optical sensors suffer from severe reading errors when applied in turbid wastewater containing particles and microbial cells. Additional, optical sensors could not achieve real-time monitoring (Ensafi et al., 2009), since long lag times (10-20 min) are needed for the color change of indicators. Disposable gold (Noh and Tothill, 2006) and single-piece nanocomposite (Liu et al., 2019) Pb(II) sensors possessed an excellent detection limit (< 10 ppb) due to the enhanced lipophilicity of sensor surface and/or the lower amount of ion exchanger in the membrane. However, a sensor surface with high lipophilicity suffered from fouling by organic/inorganic matters in water solution that severely degraded the selectivity and accuracy of ISM over time (Zhu et al., 2017). These types of sensors only had a short lifespan (less than 2 weeks in clean water solution). The N,N'-bis(salicylidene)-2,6-pyridinediamine Pb(II) sensor (Jeong et al., 2005b) had great selectivity with the only interference from K⁺ and Ag⁺ and the lifespan was about 1 month in clean water, but it had a poor detection limit (207 ppb) and did not meet the regulated Pb(II) detection requirement (< 150 ppb) in wastewater. Overall, the Pb(II) sensors reported in previous studies only meet 1-2 requirements, especially none of these sensors reported were examined in wastewater. In contrast, the S-ISM Pb(II) sensors modified using PEDOT possess all the distinct features of high accuracy/sensitivity (29 mV dec⁻¹), few interfering ion (Ag⁺), fast response time (5 s), longterm durability in wastewater (2 weeks) and low detection limit (2 ppb), ensuring the long-term continuous and accurate Pb(II) monitoring in wastewater.

3.6. Significance of our Pb(II) sensor and its energy saving in WWTPs through capturing transient Pb(II) shocks in wastewater

Existing Pb(II) electrochemical sensors sufferred from the interference of pH variations and dissolved oxygen (DO), and their fragile sensor materials and structures inhibited long-term continuous monitoring in wastewater. Miniature Pb(II) S-ISM sensor integrated with pH S-ISM sensors, equipped with a data-driven correction model, and modified using PEDOT through electropolymerization was expected to minimize these impacts. A stochastic simulation was built using Matlab to explore the improvement of the Pb(II) S-ISM sensors compared with traditional Pb(II) sensors in nitrification process (Table S2). In this model, the independent variables (pH and DO values) were randomly changed within a range (pH: 6.5-7.0, DO: 2.0 mg/L-6.0 mg/L) to simulate the real-world nitrification process, which would directly affect the output of dependent variables (the potential readings of Pb (II) S-ISM sensors). By applying the pH auto-correction data-driven model, the dependent variables would be modified automatically over time with more sensor readings fed into the model. The simulation results of 10,000 times iteration in the Matlab showed that the novel sensor assembly could effectively alleviate the errors caused by pH impact from $51 \% \sim 60 \%$ to $1\% \sim 3\%$ and alleviated the errors caused by DO

Table 1
Comparison of S-ISM Pb (II) sensors with the sensors previously reported in terms of sensitivity, selectivity, response time, long-term stability and detection limit.

Types of sensors	Sensitivity	Interfering ions	Response time	Duration test	Detection limit	Citation
This Study	28.998 mV dec ⁻¹	Ag ⁺	5 s	2 weeks in wastewater.	2 ppb	_
Commercial YSI ion-selective electrode	26 – 29mV dec [–]	Hg ²⁺ , Ag ⁺ , Cu ²⁺ , Fe ²⁺ , Cd ²⁺	5~10 s	$20 \sim 30$ min in wastewater.	20 ppb	(TruLine Lead Electrode Kit, 2020)
Disposable gold lead(II) electrode	0.9957 ug l ⁻¹	Cd ²⁺ , Ca ²⁺ , Zn ²⁺ , Hg ²⁺	~15 s	Reuse 20 times after cleaning in wastewater.	5.8 ppb	(Noh and Tothill, 2006)
Lead (II)-selective polymeric electrode based on a Schiff base complex	29.4 mV dec $^{-1}$	Cu ²⁺ , K ⁺ , Na ⁺ ,	10 s	The optimum equilibration time for the membrane electrode is 24 h.	1035 ppb	(Jeong et al., 2005a)
Optical-sensing film Pb(II) sensor	0.0072 uA dec ⁻¹	Fe ²⁺ , Fe ³⁺	~10 min	1 weeks in drinking water.	18 ppb	(Ensafi et al., 2009)
N, N'-bis(salicylidene)-2,6- pyridinediamine Pb(II) sensor	29.4 mV dec ⁻¹	K ⁺ , Ag ⁺	10 s	After one month, the electrode was responding within 95 % of the initial response in clean water// No test in wastewater.	207 ppb	(Jeong et al., 2005b)
Sol-gel lead electrode	28.9 mV dec ⁻¹	Cd ²⁺ , Cu ²⁺	10~20 s	2 months in clean water / No test in wastewater.	1035 ppb	(Ardakani et al., 2005)
Single-piece nanocomposite Pb(II) selective electrode	29.0 mV dec^{-1}	Cu ²⁺ , Ag ⁺	~10 s	2 weeks in clean water.	0.8 ppb	(Liu et al., 2019)

Table 2
Comparison of average errors from pH variations and dissolved oxygen without and with pH auto correction model and PEDOT layer in nitrification process (The simulation assumption and process were in Table S2).

	Without pH auto-correction model and PEDOT layer	With pH auto-correction model and PEDOT layer
Errors of pH from 6.5 to 7.0	51.73% ~ 60.90 %	1.21 % ~ 2.80 %
Errors of dissolved oxygen from 2.0 mg/L to 6.0 mg/L	17.3 % ~ 60.83 %	1.61 % ~ 4.86 %

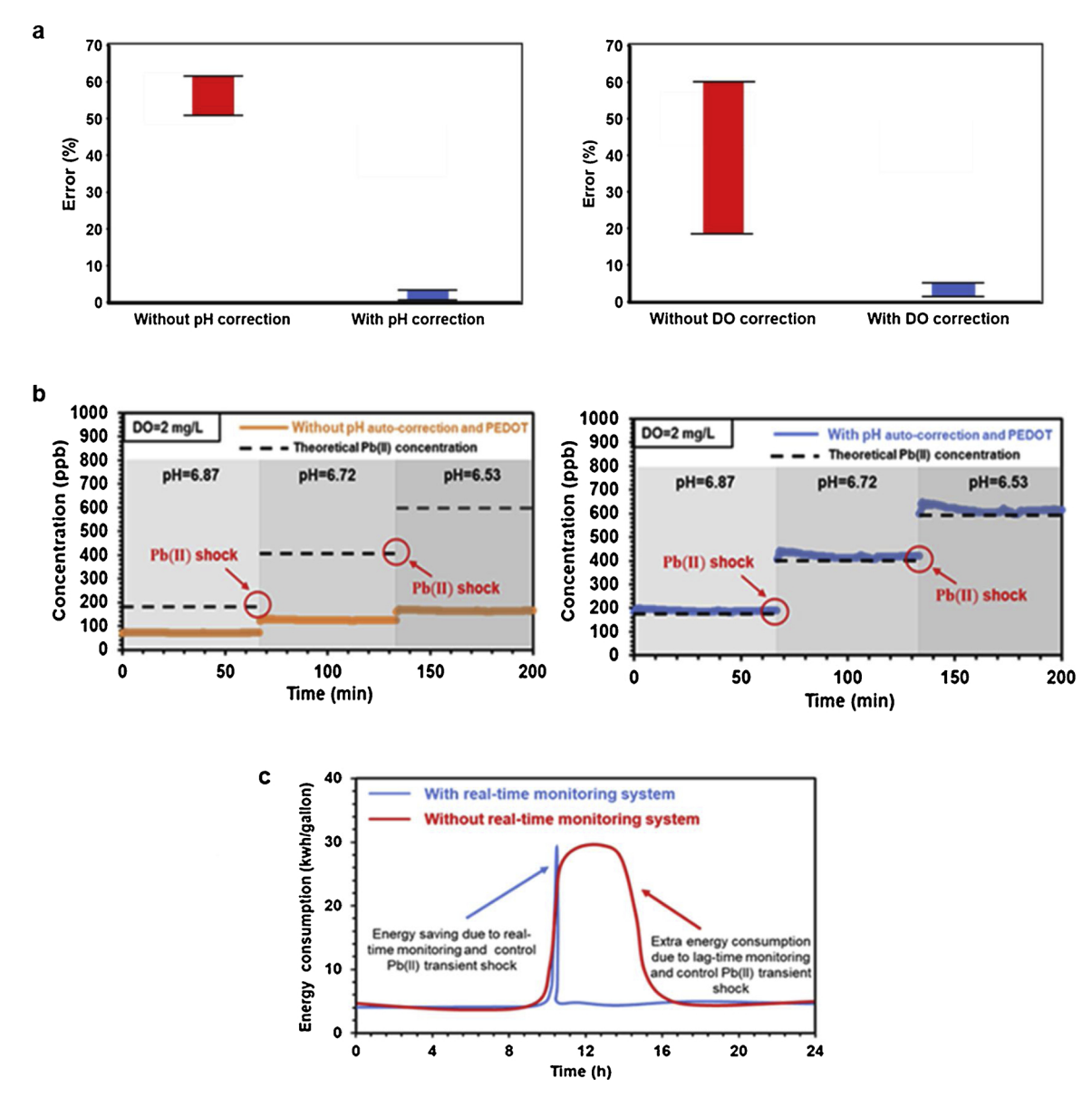


Fig. 6. (a) The result of stochastic simulation for nitrification process. (b) Validation tests of the Pb(II) S-ISM sensor with pH correction and PEDOT layer and without pH correction (as a control) under transient Pb(II) shocks in real wastewater. (c) Comparison of energy consumption with and without real-time monitoring system in a designed wastewater treatment plant.

impact from 17 % \sim 601 % to 1% \sim 5% (Table 2, Fig. 6a, Table S2).

The capability of Pb(II) S-ISM sensors to accurately capture Pb(II) transient shocks was examined by adding $Pb(NO_3)_2$ solution into real wastewater (pH: 6.87, DO: 2 mg/L), which caused an instantaneous pH fluctuation (pH: 6.72 and 6.53) monitored using a pH S-ISM sensor. The Pb(II) S-ISM sensor without the pH auto-correction model nor PEDOT layer (as the control) promptly captured transient Pb(II) shocks, but the measurement errors after two shocks were as large as 61.2 % and 64.7 %, respectively (Fig. 6b). After applying the pH auto-correction model and depositing PEDOT layer on the electrode, the measurement error was alleviated to 2.1 % and 2.5 % at pH of 6.72 and 6.53, respectively (Fig. 6b).

Based on this result, energy-saving and performance enhancement of a nitrification process with real-time *in situ* and accurate Pb(II) monitoring was extrapolated. For nitrification process in a WWTP with the capacity of 10,000 m³ per day, prompt and accurate capture Pb shocks is expected to save electricity concumption of 9.89 \times 106 kW•h (\sim 53 %) (Fig. 6c and Table S3). In contrast, conventional Pb(II) monitoring without the autocorrection model (presumably 3 h delay after Pb(II) shock) could result in the deterioated microbial activities and generate electricity consumption of 18.68 \times 106 kW•h. This clearly reveals the great potential of the mmsized Pb(II) carbon/PEDOT electrode with auto-correction data-driven model as a real-time *in situ* montioring technology.

4. Conclusion

This study aimed at tackling the critical problems of Pb(II) monitoring in water and wastewater by developing miniature solid-state ion-selective membrane (S-ISM) Pb(II) sensors with high accuracy, high selectivity and long-term durability. An innovative pH auto-correction data-driven model ($\Delta E=-2.668 \cdot pH \cdot log_{10}C_{Pb(II)} + 38.82 \cdot log_{10}C_{Pb(II)} - 26.99$) was built to overcome the complex pH inferences on Pb(II) ISM sensors. PEDOT was deposited using electropolymerization onto the mm-sized screen-printed carbon electrodes to reduce the interferences from dissolved O2 in wastewater, alleviate water penetration into the sensor entity and improve the anti-fouling property of the reference electrode. EIS and CV tests confirmed PEDOT sustained the sensor accuracy under aeration and minimized data drifting over time. The sensitivity of Pb(II) S-ISM sensors maintained at 26-29 mV per decade (close to the theoretical value) for over 2 weeks in real wastewater. Validation of the pH auto-correction model under transient Pb(II) shocks was conducted in real wastewater and the resulted clearly showed the effective of this model to minimize the measurement errors under different pH values caused by the shocks. The stochastic simulation results of 10,000 times iteration in the Matlab showed that the novel Pb(II) sensor assembly could effectively alleviate the errors caused by pH impact from 51 % \sim 61 % to 1% \sim 3% and alleviated the errors caused by DO impact from 17 % \sim 61 % to 1% \sim 5%. Thus, Monte Carlo simulation predicted that real-time in situ monitoring using Pb(II) S-ISM sensors could save 53 % energy consumption in a WWTP.

Declaration of Competing Interest

Baikun Li declares that she has no conflict of interest. The study was supported by National Science Foundation (NSF, USA).

Human Rights: This article does not contain any studies with human subjects performed by the any of the authors.

Animal studies: All institutional and national guidelines for the care and use of laboratory animals were followed.

Acknowledgements

This study was supported by National Science Foundation (NSF) Environmental Engineering Program GOALI Project (Grant No.: 1706343), NSF Partnerships for Innovation (PFI) Accelerate Innovative Research (AIR) Project (Grant No: 1640701), NSF I-Corps Project and Connecticut Biopipeline Program.

Appendix A. Supplementary data

Supplementary material related to this article can be found, in the online version, at doi:https://doi.org/10.1016/j.jhazmat.2020.123299.

References

- Andjelkovic, M., Djordjevic, A.B., Antonijevic, E., Antonijevic, B., Stanic, M., Kotur-Stevuljevic, J., Spasojevic-Kalimanovska, V., Jovanovic, M., Boricic, N., Wallace, D., Bulat, Z., 2019. Toxic effect of acute cadmium and lead exposure in rat blood, liver, and kidney. Int. J. Environ. Res. Public Health 16, 274.
- Ardakani, M.M., Kashani, M.K., Salavati-niasari, M., Ensafi, A.A., 2005. Lead ion-selective electrode prepared by sol gel and PVC membrane techniques. Sens. Actuators B Chem. 107, 438–445.
- Bansod, B.K., Kumar, T., Thakur, R., Rana, S., Singh, I., 2017. A review on various electrochemical techniques for heavy metal ions detection with different sensing platforms. Biosens. Bioelectron. 94, 443–455.
- Bobacka, J., 1999. Potential stability of all-solid-state ion-selective electrodes using conducting polymers as ion-to-electron transducers. Anal. Chem. 71, 4932–4937.
- Bobacka, J., Lewenstam, A., Ivaska, A., 2000. Electrochemical impedance spectroscopy of oxidized poly(3,4-ethylenedioxythiophene) film electrodes in aqueous solutions. J. Electroanal. Chem. 489, 17–27.
- Bruins, M.R., Kapil, S., Oehme, F.W., 2000. Microbial resistance to metals in the environment. Ecotoxicol. Environ. Saf. 45, 198–207.
- Bu, P., 1998. Carrier-based ion-selective electrodes and bulk optodes. 2. Ionophores for potentiometric and optical sensors. Chem. Rev. 98, 1593–1688.

- Changqing, L., Shuai, L., Feng, Z., 2011. The oxygen transfer efficiency and economic cost analysis of aeration system in municipal wastewater treatment plant. Energy Procedia 5, 2437–2443.
- Chua, A.S.M., Takabatake, H., Satoh, H., Mino, T., 2003. Production of polyhydroxyalkanoates (PHA) by activated sludge treating municipal wastewater: effect of pH, sludge retention time (SRT), and acetate concentration in influent. Water Res. 37, 3602–3611.
- Cohen, Y., Kirchmann, H., 2004. Increasing the pH of wastewater to high levels with different gases - CO2 stripping. Water Air Soil Pollut. 159, 265–275.
- Deng, F., Olvera-Vargas, H., Garcia-Rodriguez, O., Zhu, Y., Jiang, J., Qiu, S., Yang, J., 2019. Waste-wood-derived biochar cathode and its application in electro-Fenton for sulfathiazole treatment at alkaline pH with pyrophosphate electrolyte. J. Hazard. Mater. 377, 249–258.
- Ensafi, A.A., Far, A.K., Meghdadi, S., 2009. Highly selective optical-sensing film for lead (II) determination in water samples. J. Hazard. Mater. 172, 1069–1075.
- EPA, U., 2017. Table of Regulated Drinking Water Contaminants.
- Fibbioli, M., Morf, W.E., Badertscher, M., De Rooij, N.F., Pretsch, E., 2000. Potential drifts of solid-contacted ion-selective electrodes due to zero-current ion fluxes through the sensor membrane. Electroanalysis 12, 1286–1292.
- García-Lestón Julia, J., Méndez, J., Pásaro, E., Laffon, B., 2010. Genotoxic effects of lead: an updated review. Environ. Int. 36, 623–636.
- Guo, L., Nie, D., Qiu, C., Zheng, Q., Wu, H., Ye, P., Hao, Y., Fu, F.F., Chen, G., 2012. A G-quadruplex based label-free fluorescent biosensor for lead ion. Biosens. Bioelectron. 35, 123–127.
- Gupta, V.K., Mangla, R., Agarwal, S., 2002. Pb (II) selective potentiometric sensor based on 4- tert butylcalix [4] arene in PVC matrix. Int. J. 14, 1127–1132.
- Guziński, M., Lisak, G., Kupis, J., Jasiński, A., Bocheńska, M., 2013. Lead(II)-selective ionophores for ion-selective electrodes: a review. Anal. Chim. Acta 14, 1127–1132.
- Holenda, B., Domokos, E., Rédey, Á., Fazakas, J., 2008. Dissolved oxygen control of the activated sludge wastewater treatment process using model predictive control. Comput. Chem. Eng. 32, 1270–1278.
- Huang, M.R., Rao, X.W., Li, X.G., Ding, Y.B., 2011. Lead ion-selective electrodes based on polyphenylenediamine as unique solid ionophores. Talanta 85, 1575–1584.
- Huang, D.L., Wang, R.Z., Liu, Y.G., Zeng, G.M., Lai, C., Xu, P., Lu, B.A., Xu, J.J., Wang, C., Huang, C., 2014. Application of molecularly imprinted polymers in wastewater treatment: a review. Environ. Sci. Pollut. Res. 22, 963–977.
- Huang, J., Yuan, F., Zeng, G., Li, X., Gu, Y., Shi, L., Liu, W., Shi, Y., 2017. Influence of pH on heavy metal speciation and removal from wastewater using micellar-enhanced ultrafiltration. Chemosphere 173, 199–206.
- Jarczewska, M., Kierzkowska, E., Ziółkowski, R., Górski, Ł., Malinowska, E., 2015. Electrochemical oligonucleotide-based biosensor for the determination of lead ion. Bioelectrochemistry 101, 35–41.
- Jarosławiecka, A., Piotrowska-Seget, Z., 2014. Lead resistance in micro-organisms. Microbiology 160, 12–25.
- Jenner, G.A., Longerich, H.P., Jackson, S.E., Fryer, B.J., 1990. ICP-MS A powerful tool for high-precision trace-element analysis in Earth sciences: evidence from analysis of selected U.S.G.S. reference samples. Chem. Geol. 83, 133–148.
- Jeong, T., Jeong, D.C., Hyo, K.L., Jeon, S., 2005a. Lead(II)-selective polymeric electrode using a Schiff base complex of N,N'-bis-thiophene-2-ylmethylene-ethane-1,2-diamine as an ion carrier. Bull. Korean Chem. Soc. 26, 1219.
- Jeong, T., Lee, H.K., Jeong, D.C., Jeon, S., 2005b. A lead(II)-selective PVC membrane based on a Schiff base complex of N,N'-bis(salicylidene)-2,6-pyridinediamine. Talanta 65, 543–548.
- Jiang, W., Liu, C., Zhao, Y., Waterhouse, G.I.N., Zhang, Z., Yu, L., 2019. A solid-contact Pb 2+ -selective electrode based on a hydrophobic polyaniline microfiber film as the ion-to-electron transducer. Synth. Met. 248, 94–101.
- Kalluri, J.R., Arbneshi, T., Khan, S.A., Neely, A., Candice, P., Varisli, B., Washington, M., McAfee, S., Robinson, B., Banerjee, S., Singh, A.K., Senapati, D., Ray, P.C., 2009. Use of gold nanoparticles in a simple colorimetric and ultrasensitive dynamic light scattering assay: selective detection of arsenic in groundwater. Angew. Chemie Int. Ed. 48, 9669-9671.
- Kang, W., Pei, X., Rusinek, C.A., Bange, A., Haynes, E.N., Heineman, W.R., Papautsky, I., 2017. Determination of lead with a copper-based electrochemical sensor. Anal. Chem. 89, 3345–3352.
- Kaur, K., Aulakh, J.S., 2018. Analytical & bioanalytical techniques fabrication of Pb (II) selective polymeric membrane electrode based on 2, 2'[Propane-1, 3-Diylbis (oxy)] dibenzaldehyde as an ionophore. J. Anal. Bioanal. Technol. 9, 2.
- Khan, A.A., Khan, M.Q., Shaheen, S., 2016. Synthesis, characterization, and electroanalytical studies of Pb2+-selective polypyrrole-Zr(IV) phosphate ion exchange membrane. J. Solid State Electrochem. 20, 2079–2091.
- Kühr, S., Schneider, S., Meisterjahn, B., Schlich, K., Hund-Rinke, K., Schlechtriem, C., 2018. Silver nanoparticles in sewage treatment plant effluents: chronic effects and accumulation of silver in the freshwater amphipod Hyalella azteca. Environ. Sci. 30. 7.
- Kulesza, J., Bocheńska, M., 2011. Calixthioamides as ionophores for transition- and heavy-metal cations. Eur. J. Inorg. Chem. 2011, 777–783.
- Lee, C., Choi, S.W., Lee, I.B., 2006. Sensor fault diagnosis in a wastewater treatment process. Water Sci. Technol. 53, 251–257.
- Li, X.G., Ma, X.L., Huang, M.R., 2009. Lead(II) ion-selective electrode based on polyaminoanthraquinone particles with intrinsic conductivity. Talanta 78, 498–505.
- Li, F., Feng, Y., Zhao, C., Tang, B., 2011. Crystal violet as a G-quadruplex-selective probe for sensitive amperometric sensing of lead. Chem. Commun. 47, 11909–11911.
- Li, M., Liu, J., Han, W., 2016. Recycling and management of waste lead-acid batteries: a mini-review. Waste Manage. Res. 34, 298–306.
- Lisak, G., Bobacka, J., Lewenstam, A., 2012. Recovery of nanomolar detection limit of solid-contact lead (II)-selective electrodes by electrode conditioning. J. Solid State

- Electrochem. 16, 2983-2991.
- Lisak, G., Kupis, J., Jasi, A., Boche, M., 2013. Lead (II) -selective ionophores for ionselective electrodes: a review. Anal. Chim. Acta 791, 1–12.
- Liu, Yueling, Liu, Yang, Gao, Y., Wang, P., 2019. A general approach to one-step fabrication of single-piece nanocomposite membrane based Pb 2+ -selective electrodes. Sens. Actuators B Chem. 281, 705–712.
- Marani, D., Macchi, G., Pagano, M., 1995. Lead precipitation in the presence of sulphate and carbonate: testing of thermodynamic predictions. Water Res. 29, 1085–1092.
- Meng, Q., Cai, K., Chen, Y., Chen, L., 2017. Research progress on conducting polymer based supercapacitor electrode materials. Nano Energy 36, 268–285.
- Moon, J.M., Thapliyal, N., Hussain, K.K., Goyal, R.N., Shim, Y.B., 2018. Conducting polymer-based electrochemical biosensors for neurotransmitters: a review. Biosens. Bioelectron. 102, 540–552.
- Naveen, M.H., Gurudatt, N.G., Shim, Y.B., 2017. Applications of conducting polymer composites to electrochemical sensors: a review. Appl. Mater. Today 9, 419–433.
- Noh, M.F.M., Tothill, I.E., 2006. Development and characterisation of disposable gold electrodes, and their use for lead(II) analysis. Anal. Bioanal. Chem. 386, 2095–2106.
- Pechenkina, I.A., Mikhelson, K.N., 2015. Materials for the ionophore-based membranes for ion-selective electrodes: problems and achievements (review paper). Russ. J. Electrochem. 51, 93–102.
- Polk, B.J., Stelzenmuller, A., Mijares, G., MacCrehan, W., Gaitan, M., 2006. Ag/AgCl microelectrodes with improved stability for microfluidics. Sens. Actuators B Chem. 114, 239–247.
- Püntener, M., Vigassy, T., Baier, E., Ceresa, A., Pretsch, E., 2004. Improving the lower detection limit of potentiometric sensors by covalently binding the ionophore to a polymer backbone. Anal. Chim. Acta 503, 187–194.
- Rajkumar, D., Song, B.J., Kim, J.G., 2007. Electrochemical degradation of Reactive Blue 19 in chloride medium for the treatment of textile dyeing wastewater with identification of intermediate compounds. Dyes Pigm. 72, 1–7.
- Rangreez, T.A., Inamuddin, 2016. Synthesis and characterization of graphene Th(IV) phosphate composite cation exchanger: analytical application as lead ion-selective membrane electrode. Desalin. Water Treat. 57, 23893–23902.
- Rozendal, R.A., Sleutels, T.H.J.A., Hamelers, H.V.M., Buisman, C.J.N., 2008. Effect of the type of ion exchange membrane on performance, ion transport, and pH in biocatalyzed electrolysis of wastewater. Water Sci. Technol. 57, 1757–1762.
- Sari, A., Tuzen, M., Citak, D., Soylak, M., 2007. Equilibrium, kinetic and thermodynamic

- studies of adsorption of Pb(II) from aqueous solution onto Turkish kaolinite clay. J. Hazard. Mater. 149, 283–291.
- Shi, H., Liu, C., Jiang, Q., Xu, J., 2015. Effective approaches to improve the electrical conductivity of PEDOT:PSS: a review. Adv. Electron. Mater. 1, 1500017.
- Triantafyllidou, S., Edwards, M., 2012. Lead (Pb) in tap water and in blood: implications for lead exposure in the United States. Crit. Rev. Environ. Sci. Technol. 42, 1297–1352
- TruLine Lead Electrode Kit, 2020. https://www.ysi.com/Product/id-400416/TruLine-Lead-Electrode-Kit.
- Wang, Y., 2009. Research progress on a novel conductive polymer-poly(3,4- ethylene-dioxythiophene) (PEDOT). J. Phys. Conf. Ser. 152, 12023.
- Wang, Yyan, Chai, Lyuan, Chang, H., Peng, Xyu, Shu, Yde, 2009. Equilibrium of hydroxyl complex ions in Pb2+-H2O system. Trans. Nonferrous Met. Soc. China 19, 458–462.
- Yang, Xiaoyun, et al., 2012. Prevention of electrode fouling can significantly improve an accuracy of tricresyl phosphate detection. ECS Meet. Abstr. 46, 1649.
- Yang, Y., Lee, E.K., Surowiec, K., Bartsch, R.A., 2015. Di-ionizable p-tert-butylcalix[4] arene-1,2-crown-5 ligands in the cone conformation: effect of acidic side arm length for solvent extraction of divalent metal ions. Tetrahedron 71, 77–84.
- Yu, S., Li, F., Yin, T., Liu, Y., Pan, D., Qin, W., 2011. A solid-contact Pb2+-selective electrode using poly(2-methoxy-5-(2'-ethylhexyloxy)-p-phenylene vinylene) as ionto-electron transducer. Anal. Chim. Acta 702, 195–198.
- Yu, L., Zhang, P., Dai, H., Chen, L., Ma, H., Lin, M., Shen, D., 2017. An electrochemical sensor based on Co3O4 nanosheets for lead ions determination. RSC Adv. 7, 39611–39616
- Zhao, L., Zhong, S., Fang, K., Qian, Z., Chen, J., 2012. Determination of cadmium(II), cobalt(II), lickel(II), lead(II), zinc(II), and copper(II) in water samples using dual-cloud point extraction and inductively coupled plasma emission spectrometry. J. Hazard. Mater. 239, 206–212.
- Zhu, Z., Jiang, J., Wang, X., Huo, X., Xu, Y., Li, Q., Wang, L., 2017. Improving the hydrophilic and antifouling properties of polyvinylidene fluoride membrane by incorporation of novel nanohybrid GO@SiO2 particles. Chem. Eng. J. 314, 266–276.
- Zou, J., Wu, S., Liu, Y., Sun, Y., Cao, Y., Hsu, J.P., Shen Wee, A.T., Jiang, J., 2018. An ultra-sensitive electrochemical sensor based on 2D g-C3N4/CuO nanocomposites for dopamine detection. Carbon 130, 652–663.
- Zou, J., Mao, D., Arramel, Li, N., Jiang, J., 2020. Reliable and selective lead-ion sensor of sulfur-doped graphitic carbon nitride nanoflakes. Appl. Surf. Sci. 506, 144672.